Scale-free topology of vortical networks in a turbulent thermoacoustic system

Jianyi Zheng●

School of Mechanical Engineering, Shanghai Jiao Tong University, 800 Dong Chuan Road, Minhang, Shanghai 200240, China

Yu Guan●

Department of Aeronautical and Aviation Engineering, The Hong Kong Polytechnic University, Kowloon, Hong Kong

Liangliang Xu● and Xi Xia●

School of Mechanical Engineering, Shanghai Jiao Tong University, 800 Dong Chuan Road, Minhang, Shanghai 200240, China

Larry K. B. Li●[*]

Department of Mechanical and Aerospace Engineering, The Hong Kong University of Science and Technology, Clear Water Bay, Hong Kong

Fei Qi●

School of Mechanical Engineering, Shanghai Jiao Tong University, 800 Dong Chuan Road, Minhang, Shanghai 200240, China

We use complex network analysis to investigate the vortical interactions in a bluff-body stabilized combustion system containing a turbulent lean premixed swirling flame. Using time-resolved vorticity measurements, we construct time-varying weighted spatial networks whose node strength distribution is derived from the Biot-Savart law. We find widespread evidence of scale-free topology in the vortical networks, with the most coherent flow structures acting as the primary network hubs. Crucially, we find that even after the onset of thermoacoustic instability, the scale-free topology can persist continuously in time, contrary to some suggestions from the literature. This discovery could have important implications for the design of flow controllers that rely on destroying the primary hubs of vortical networks.

I. INTRODUCTION

Lean premixed combustion is known to be able to lower thermal NOx emissions from gas turbines. Such systems typically contain a swirling flame whose stability against high-speed reactants is provided by high-temperature recirculation zones [1,2]. However, lean premixed combustion is also known to be prone to thermoacoustic instability [3]. This self-excited phenomenon can cause intense pressure oscillations to arise in gas turbine combustors, limiting their efficiency, operability, and reliability [4,5].

---

[*]larryli@ust.hk

033202-1

Previous studies have shown that coherent vortices generated from the injector lip of a combustor can cause flames to respond nonlinearly to incident flow perturbations [1]. Such vortical structures can induce flame roll-up, cusp formation, and surface annihilation, causing further fluctuations in the heat release rate (HRR) [6]. Palies *et al.* [7] showed that the interactions between vortex roll-up and flame angle oscillations can influence the local minimum and maximum gain values of the transfer function of a swirling flame. The crucial role of vortical structures was further highlighted by Oberleithner *et al.* [8], who used linear stability analysis to show that the shear layer receptivity correlates well with the flame transfer function. For both bluff-body and aerodynamically stabilized swirling flames, Gatti *et al.* [9] found that the flame transfer function is strongly dependent on the large-scale vortical structures shed from the injector lip. From these and other related studies [1,2], it is now clear that the accurate prediction and control of thermoacoustic oscillations requires a thorough understanding of the flame response under vortical modulation.

In the past several decades, complex networks have emerged as a powerful tool with which to understand and control the spatiotemporal dynamics of complex systems in various fields of science and engineering [10–12]. In network analysis, the components of a system are treated as nodes, while their interactions are treated as links. If the links of a network exhibit a heavy-tailed distribution with no characteristic scale, then that network is said to be scale free [13]. In the node degree distribution, such scale-free topology can be identified by a power-law scaling of the form $P(k) \sim k^\gamma$, where $P(k)$ is the percentage of nodes with k links to other nodes and γ has a typical value between -2 and -3 [14]. Such a power-law scaling, which is caused by nodal growth and preferential attachment [13], implies that most nodes have only a small number of links, but that a few nodes have a disproportionately large number of links. The latter nodes, called hubs, play a critical role in dictating the behavior of the entire network and are thus particularly susceptible to control action [12,15].

In thermoacoustics, network analysis has been gaining traction recently, following seminal experiments by Murugesan and Sujith [16] and Okuno *et al.* [17] showing that the onset of thermoacoustic instability is often presaged by a loss of scale-free topology in complex networks built with pressure data. This discovery has since inspired fresh approaches to the early detection of thermoacoustic instability. For example, using a visibility algorithm, Murugesan and Sujith [18] built complex networks from pressure time-series data collected on a turbulent lean premixed combustor. They found evidence of scale-free topology during both a low-amplitude aperiodic state of combustion noise (high-dimensional deterministic chaos [19]) and a medium-amplitude transitional state of intermittency. However, they found that the scale-free topology is replaced by an ordered structure when the system transitions from intermittency to a high-amplitude self-excited state of thermoacoustic instability (limit-cycle dynamics). Crucially, this loss of scale-free behavior was observed to be gradual rather than abrupt. This made it possible to derive precursors of thermoacoustic instability based on various network metrics, such as the network diameter, characteristic path length, and clustering coefficient [18].

Meanwhile, evidence has emerged that for complex networks built with vorticity data rather than pressure data, the scale-free topology that is expected to disappear at the onset of thermoacoustic instability survives to some degree. For example, Murayama *et al.* [20] adopted the vortical-interaction framework of Taira *et al.* [21] to build turbulence networks with vorticity data from a swirl-stabilized combustor. They found that even after becoming thermoacoustically unstable, the combustor can still exhibit scale-free network topology for around one-fifth of the operating time. Similarly, Krishnan *et al.* [22] built time-varying weighted spatial networks with turbulent flow-field data from a bluff-body stabilized combustor. They found that the node strength distribution only intermittently exhibits a power-law scaling with $-3 < \gamma < -2$, indicating that scale-free topology appears only some of the time. In particular, those observations of scale-free topology were found to be less frequent during intermittency and thermoacoustic instability than during combustion noise. The scale-free behavior was attributed to two sets of large-scale coherent vortical structures, one downstream of the dump plane and the other downstream of the bluff body. Those vortical structures were determined to be the primary hubs of the turbulence network, dictating the spatiotemporal
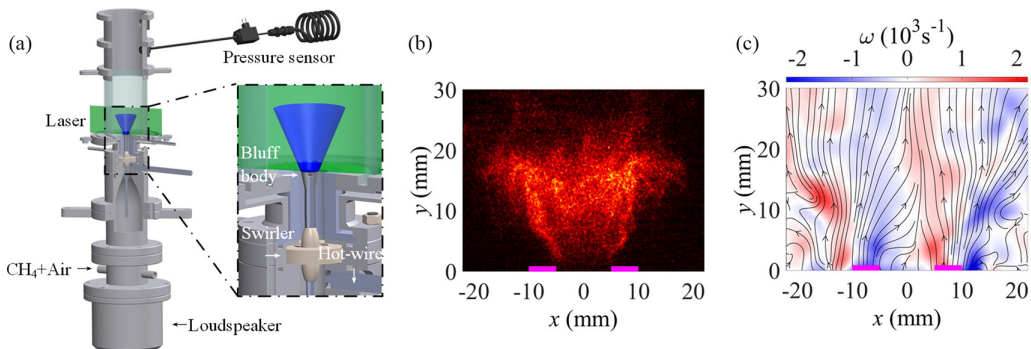
FIG. 1. (a) Illustration of the experimental setup; for details, see Wang *et al.* [28] and Zheng *et al.* [29]. Also shown are instantaneous snapshots of the (b) CH* chemiluminescence and (c) vorticity fields of the flame during a thermoacoustically stable state in which acoustic forcing is applied at a frequency of $f_f = 183$ Hz and an amplitude of $u'/\bar{u} = 0.1$. In (b) and (c), the magenta lines at the bottom represent the burner outlet. In (c), the black lines are streamlines.

dynamics of the entire flow even after the onset of thermoacoustic instability [22]. Thus, disrupting those primary network hubs—via the injection of steady air jets in regions of high vorticity—has been shown to be an effective way of suppressing thermoacoustic instability [22–24]. Collectively, these studies have demonstrated that in the analysis of thermoacoustic systems, vortical networks can exhibit far more intricate features than pressure networks. However, the precise influence of vortical structures on the network properties during both forced modulation and self-excited thermoacoustic instability remains an unresolved question. This question is nonetheless important within the thermoacoustics community, as it aims to enhance the understanding of self-organized dynamics through a comparative analysis with forced dynamics. Complicating the matter further is the fact that the onset of thermoacoustic instability coincides with the mutual synchronization of the pressure and HRR signals [25–27]. In turbulent combustors, the HRR field of a flame is known to be strongly correlated with the vorticity field of the underlying injector flow, indicating a nontrivial relationship between pressure and vortical networks. Gaining a better understanding of this relationship could therefore provide the key to unlocking the flame–acoustic coupling mechanisms behind thermoacoustic instability.

In this experimental study, we apply complex network analysis to the time-resolved pressure and vorticity fields of a turbulent lean premixed combustor containing a bluff-body stabilized swirling flame. Our aim is to better understand the vortical interactions in the reacting flow field by relating the scale-free topology of the vortical networks to the pressure dynamics in the combustor. To this end, we consider three canonical states: (i) an unforced state of combustion noise, (ii) an acoustically forced state without thermoacoustic instability, and (iii) a thermoacoustically self-excited state.

II. EXPERIMENTAL SETUP AND TEST CONDITIONS

Our experimental setup is identical to that of Wang *et al.* [28] and Zheng *et al.* [29]. Shown in Fig. 1(a), it consists of a confined turbulent lean premixed flame produced by feeding air and methane (CH_4) into a settling chamber via mass flow controllers (SevenStar CS200A). The chamber contains an axial flow swirler (a swirl number of 0.6), with a conical bluff body mounted at the burner outlet for flame holding. The burner outlet is thus annular, with outer and inner diameters of $d_o = 20$ and $d_i = 10$ mm, respectively. Connected downstream is a cylindrical quartz combustor (length 475 mm, inner diameter 76 mm), which provides acoustic feedback for thermoacoustic instability to arise under certain flow conditions (see below). For some test cases, a loudspeaker mounted upstream of the settling chamber is used to generate sinusoidal acoustic forcing, and the resultant velocity perturbations are measured with a hot-wire anemometer (Dantec MiniCTA)

mounted upstream of the axial swirler. The forcing amplitude is defined as $u'/\bar{u}$, where u' and $\bar{u}$ are the velocity fluctuation amplitude and the time-averaged velocity, respectively. The time-resolved spatial distribution of flow velocity in the combustor is measured along the central plane using two-dimensional particle image velocimetry (PIV). Specifically, dual burst-mode Nd:YAG lasers (Spectral Energies QuasiModo 1000.2X) are operated at a frequency of 20 kHz, generating pulses of 10 ns in duration and 250 mJ in energy at a wavelength of 532 nm. The two laser beams are expanded into an overlapping planar sheet via a series of optics. The light scattered from seeding particles (Al_2O_3, with a nominal diameter of 1 micron) is captured with a high-speed CMOS camera (Photron FASTCAM SA-Z) equipped with a bandpass optical filter (Edmund Optics 532/10 nm).

Simultaneously, the acoustic pressure (p') in the combustor is measured at 100 kHz using a piezoelectric sensor (Sinocera CY-YD-200) mounted 161 mm downstream of the burner outlet via the semi-infinite tube method. For the unforced and forced states, which are both free of thermoacoustic instability, the reactants have a velocity of $\bar{u} = 5\,\mathrm{m\,s^{-1}}$ and an equivalence ratio of $\phi = 0.8$ (lean combustion), giving a Reynolds number of $\mathrm{Re} = 2600$ based on d_o. Figures 1(b) and 1(c) show, respectively, instantaneous snapshots of the CH^* chemiluminescence and vorticity fields of the flame during the forced state. It can be seen that even under acoustic excitation, the flame remains anchored to the bluff body, with most of its HRR occurring in the central wake region between the inner shear layers, where strong vorticity exists. To induce a thermoacoustically self-excited state, we increase $\bar{u}$ to $12\,\mathrm{m\,s^{-1}}$, while keeping ϕ between 0.7 and 0.8, resulting in $\mathrm{Re} = 6200$. Further details on the experimental set-p and procedures can be found in Wang *et al.* [28] and Zheng *et al.* [29].

III. RESULTS AND DISCUSSION

We use network analysis to examine the complex dynamics hidden in the pressure and vorticity data. As noted earlier, we focus on three representative states: an unforced state, an acoustically forced state, and a thermoacoustically self-excited state. We first characterize the pressure signals using graph theory, then explore the scaling properties of the node strength distribution of turbulence networks constructed from the vorticity field, and finally compare the temporal evolution of those scaling properties with that of the pressure signals.

A. Network analysis of the pressure signal

First, we characterize the dynamical state of the system by analyzing the temporal structures in the p' signal. Figures 2(a1)–2(c1) show the p' signal, and Figs. 2(a2)–2(c2) show the corresponding power spectral density (PSD) for all three states. In the unforced state (Fig. 2, top row), the system exhibits only low-amplitude aperiodic p' fluctuations, with no dominant peaks in the PSD. This indicates a state of combustion noise dominated by chaotic turbulence, free of the tonal nature of thermoacoustic instability. In the forced state (Fig. 2, middle row), the system is still thermoacoustically stable, but the p' signal is now periodic as a result of the applied forcing, with the system behaving as a forced damped oscillator. Here, the forcing is applied sinusoidally at a frequency of $f_f = 183\,\mathrm{Hz}$ and an amplitude of $u'/\bar{u} = 0.2$, producing periodic p' oscillations of a moderate amplitude. In phase space, this state could be regarded as a closed periodic orbit similar to a limit-cycle attractor. We then increase Re from 2600 to 6200 to produce a thermoacoustically self-excited state with high-amplitude periodic p' oscillations (Fig. 2, bottom row). The PSD is dominated by an energetic peak at 310 Hz with a weaker subharmonic, indicating that thermoacoustic instability in this system takes the form of a quarter-wave mode. This is the intrinsic thermoacoustic mode identified previously by Xu *et al.* [30].

Next, we analyze the p' signal using the horizontal visibility graph (HVG), a graph-theoretical tool for mapping time-domain data to network structures [31]. We use a filtered version of the HVG capable of detecting hidden periodicity even in signals corrupted by noise, enabling stochastic, chaotic, and noisy periodic dynamics to be distinguished [32]. Figures 2(a3)–2(c3) show the mean
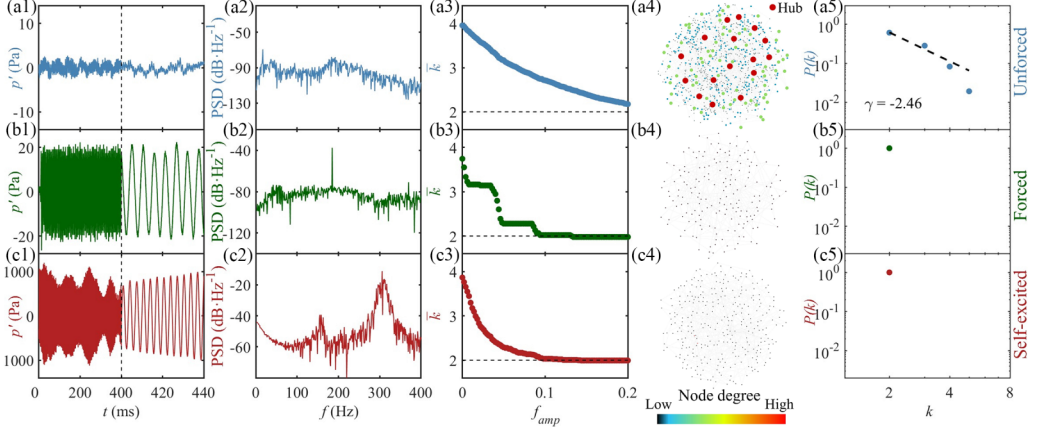
FIG. 2. System dynamics based on the pressure fluctuation signal p' for three representative states: (a1)–(a5) unforced state of combustion noise, (b1)–(b5) acoustically forced state without thermoacoustic instability, and (c1)–(c5) thermoacoustically self-excited state. From left to right, the columns show the time trace of p' (note the change in timescale at $t = 400$ ms), the PSD of p', the HVG mean degree vs the graph-theoretical noise filter amplitude, the network structure with the highest degree nodes (hubs) shown as red dots, and the node degree distribution.

degree $\bar{k}$—the mean number of nodes linked to a given node—as a function of f_{amp}, the amplitude of the graph-theoretical noise filter. For a perfectly sinusoidal signal without any noise, $\bar{k} \to 2$ because all the network nodes are linked only to their immediate neighbors. In the unforced state [Fig. 2(a3)], the system dynamics are aperiodic, dominated by chaotic turbulence. This prevents $\bar{k}$ from converging to 2, even when f_{amp} reaches a high value (0.2). The network structure [Fig. 2(a4)] contains several nodes with a disproportionately large number of links. These high-degree nodes are the network hubs and are highlighted as red dots. The node degree distribution [Fig. 2(a5)] shows a power-law scaling with an exponent of $\gamma = -2.46$, indicating that the topology of the pressure network is scale free. This finding is consistent with that of Murugesan and Sujith [16] and Murayama et al. [20]. For both the forced and self-excited states [Figs. 2(b3) and 2(c3)], $\bar{k}$ converges to exactly 2 as f_{amp} increases. This confirms the dominance of periodic dynamics, with increases in f_{amp} acting to filter out the effects of small-scale turbulence. For the forced state [Fig. 2(b3)], $\bar{k}$ experiences abrupt drops as f_{amp} increases; these drops are due to harmonic disturbances generated by the forcing. For both states [Figs. 2(b4), 2(b5) and Figs. 2(c4), 2(c5)], the network structure contains no hubs, with the node degree distribution collapsing to a single point, indicating a complete loss of scale-free topology in the pressure networks. Again, these findings are consistent with previous studies [27], further substantiating our methodology.

B. Network analysis of the vorticity field

Having examined the pressure dynamics, we now turn to the vorticity dynamics as captured by time-resolved PIV (see Sec. II). We perform a time-varying weighted network analysis based on the framework of Taira et al. [21]. This involves constructing, at each time instant, a spatial network whose nodes represent fluid elements that induce a velocity at other fluid elements via the vorticity field (ω). The velocity magnitude induced by fluid element i on another fluid element j is found via the Biot-Savart law,

$$u_{i \to j} = \frac{|\gamma_i|}{2\pi \sqrt{(x_i - x_j)^2 + (y_i - y_j)^2}}, \tag{1}$$
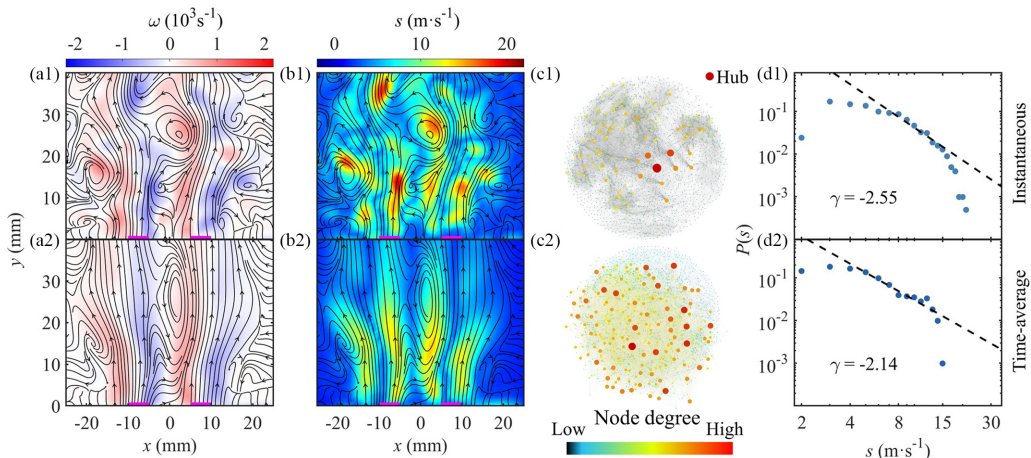
FIG. 3. Unforced state of combustion noise (Re = 2600, $\phi = 0.8$): (a1),(a2) vorticity field, (b1),(b2) node strength field from vortical networks, (c1),(c2) network structure with the highest strength nodes (hubs) shown as red dots, and (d1),(d2) node strength distribution on a log-log plot. Both the instantaneous and time-averaged data are shown. In the spatial data [(a1),(a2) and (b1),(b2)], the black lines are streamlines and the magenta lines at the bottom represent the burner outlet.

where $\gamma_i = \omega(x_i, y_i)\Delta x \Delta y$ is the circulation of element i whose width and length are Δx and Δy, respectively. Here the vorticity ω is the out-of-plane component provided by our two-dimensional PIV measurements (Sec. II). This component is used because our previous dual-plane stereoscopic PIV measurements revealed that the dominant vortical structures in the present flow field are the outer vortex rings [29]. These rings are axisymmetric, producing a high concentration of out-of-plane vorticity when the PIV laser sheet is aligned along the central plane [Fig. 1(a)]. The magnitude of the average induced velocity is assigned to the weight A_{ij} of the link between fluid elements i and j, providing an instantaneous measure of their vortical interaction strength. For an entire network, this is encapsulated by the adjacency matrix,

$$A_{ij} = \begin{cases} \frac{1}{2}(u_{i \to j} + u_{j \to i}) & \text{if} \quad i \neq j, \\ 0 & \text{if} \quad i = j. \end{cases} \tag{2}$$

This type of vortical network is considered a complete graph because each element interacts with every other element. The node strength ($s_i \equiv \sum_{j=1}^{N} A_{ij}$), which is defined as the sum of all the weights (A_{ij}) at a given element (node i), is an indicator of how strongly that node interacts with all N nodes of the network. Physically, an increase in s_i implies an increase in the velocity induced by fluid element i on all the other fluid elements [21,22]. To determine the network topology, we examine the node strength distribution $P(s)$, which is the percentage of nodes with strength s. If a power-law scaling of the form $P(s) \sim s^{\gamma}$ with $-3 < \gamma < -2$ is observed, then the network is considered to be scale free [14]. In a scale-free network, the weight distribution of the links is highly inhomogeneous, with most nodes exhibiting small s. However, a few nodes exhibit disproportionately large s, making them hubs. Such a network is termed scale free because nodes with a wide range of s values coexist with no characteristic scale. Below we use such a weighted spatial network analysis to investigate the vortical interactions in our combustion system for the three states examined in Sec. III A.

1. Unforced state of combustion noise

Figure 3 shows the spatial distributions of ω and s alongside the network structure and $P(s)$, all for the unforced state. From both instantaneous and time-averaged data, we find that the high $|\omega|$

regions overlap with the high s regions, confirming that the node strength can reliably capture the dominant vortical structures. We also find that for this thermoacoustically stable state dominated by combustion noise (high-dimensional deterministic chaos [19]), the node strength distribution follows the power-law scaling $P(s) \sim s^\gamma$ with $-3 < \gamma < -2$ for almost every sampled time instant, indicating that these vortical networks are almost continuously scale free, regardless of the phase of development of the coherent flow structures. This assessment is confirmed by the presence of hubs of high node strength in the network structure [Figs. 3(c1), 3(c2)]. Our observation of scale-free topology in vortical networks at nearly all times during a state of combustion noise is consistent with that of Murayama *et al.* [20] and Krishnan *et al.* [22]. The observation is also consistent with the experiments of Murayama *et al.* [33], who found that the scale-free existence probability for an unforced thermoacoustically stable system exhibits a narrow Gaussian distribution. The coherent flow structures with high $|\omega|$ near the inner and outer shear layers are the primary hubs of the vortical networks [Figs. 3(a1), 3(a2) and Figs. 3(b1), 3(b2)], dominating the spatiotemporal dynamics of the entire flow. We find that time averaging the data smears the ω distribution, reducing the strength of those vortical structures and thus reducing γ; nevertheless, scale-free topology still persists [Figs. 3(c1), 3(c2) and Figs. 3(d1), 3(d2)].

2. Forced state without thermoacoustic instability

Figure 4 is analogous to Fig. 3, but for the forced state. Instead of showing the instantaneous and time-averaged data, we show the phase-averaged data at five instants in a forced oscillation cycle, with each instant separated in time by an angle of $2\pi/5$. Here a phase angle of 0 corresponds to the moment when an outer vortex ring is generated at the burner outlet. This moment precedes the moment of minimum acoustic pressure by a small angle [0.127π; see Fig. 5(c2)]. We find that energetic coherent vortices are shed periodically from the burner lip, in synchronization with the periodic velocity perturbations arising from the applied forcing. These acoustically induced vortices act as the primary network hubs, dominating the entire flow. In the node strength distribution [Figs. 4(d1)–4(d5)], we find clear evidence of a power-law scaling, but γ always remains below -3, indicating that these vortical networks are in the random regime rather than in the scale-free regime, as defined by Barabási [14]. We find that γ depends on the spatiotemporal development of the vortical structures. As the vortices in the outer shear layers emerge and grow (phase angle $0 \rightarrow 4\pi/5$), γ increases, indicating a more even distribution of s. Then, as those vortices begin to dissipate (phase angle $4\pi/5 \rightarrow 8\pi/5$), γ decreases, causing the networks to move further into the random regime.

We find that the range of values in which γ fluctuates depends on f_f. To illustrate this, we show in Fig. 5 the temporal evolution of γ for three different forcing frequencies ($f_f = 63, 133,$ and 183 Hz), all at the same forcing amplitude ($u'/\bar{u} = 0.2$). This range of f_f was chosen based on a balance between exploiting the low-pass filtering characteristics of the HRR response of the flame [34] and exciting the system at frequencies close to the fundamental or subharmonic of the incipient self-excited thermoacoustic mode (Fig. 2 and Sec. III B 3). The case of $f_f = 183$ Hz was examined in Fig. 4. For both instantaneous and phase-averaged data (Fig. 5), we find that γ increases as f_f decreases. At the lowest f_f value (63 Hz), γ even intermittently enters the scale-free range ($-3 < \gamma < -2$), which is reminiscent of the intermittent scale-free dynamics observed by Krishnan *et al.* [22] in vortical networks during intermittency and thermoacoustic instability. In our case, the change in γ may be due to a decrease in the vortex core energy with decreasing f_f [34]. The instantaneous γ data are seen to fluctuate more than the phase-averaged data because turbulence causes ω to be more scattered and randomly distributed. Figure 5 also shows the temporal evolution of p' in relation to that of γ. Regardless of f_f, we find that these two signals are well correlated, indicating that the hydrodynamic field is strongly receptive to the applied forcing. This is in line with the spatial amplifier characteristics of a convectively unstable flow [35]. In summary, we have shown that the degree of scale-free topology in vortical networks built from a forced turbulent combustion system without thermoacoustic instability is highly dependent on the presence and
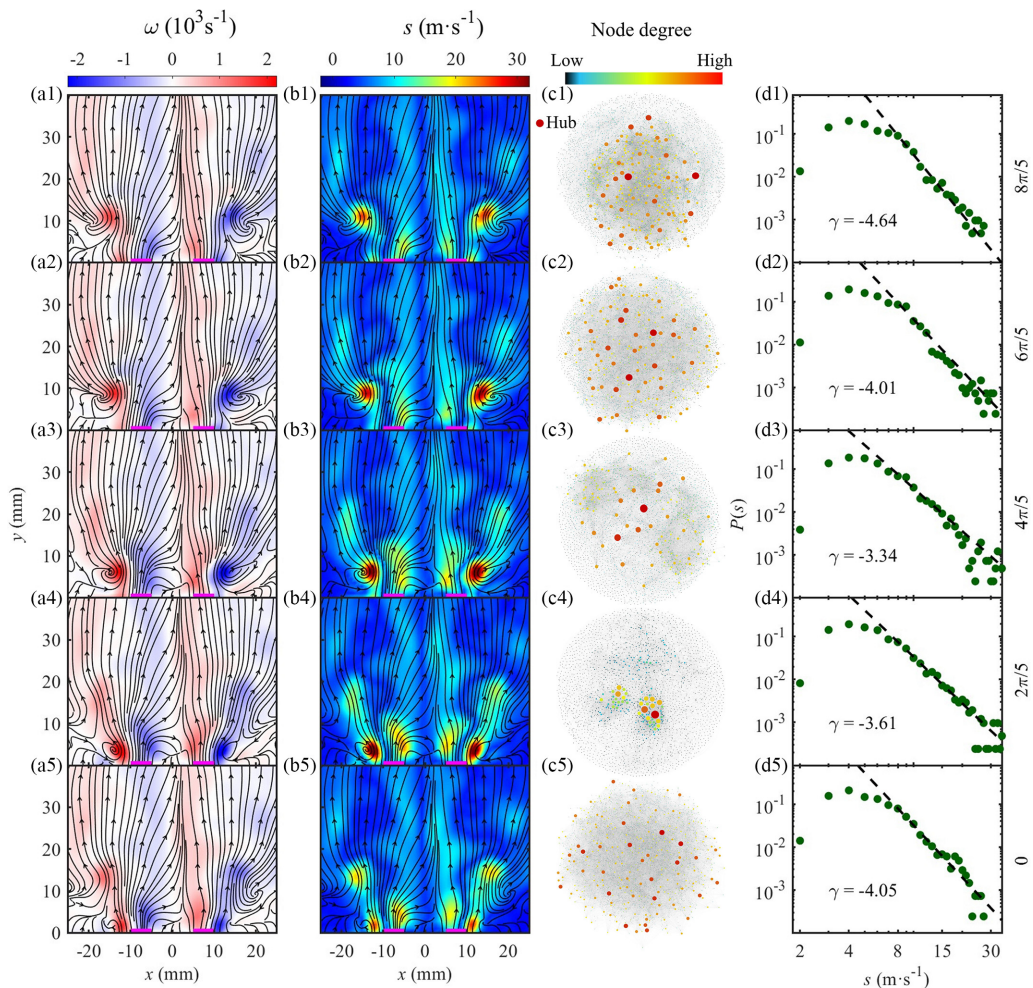
FIG. 4. Forced state without thermoacoustic instability (Re = 2600, $\phi = 0.8$): (a1)–(a5) vorticity field, (b1)–(b5) node strength field from vortical networks, (c1)–(c5) network structure with the highest strength nodes (hubs) shown as red dots, and (d1)–(d5) node strength distribution on a log-log plot. The data shown are phase averaged at five instants in a forced oscillation cycle, with each instant separated from the next by an angle of $2\pi/5$ (see labels on the right). The forcing is applied at a frequency of $f_f = 183$ Hz and an amplitude of $u'/\bar{u} = 0.2$. In the spatial data [(a1)–(a5), (b1)–(b5)], the black lines are streamlines and the magenta lines at the bottom represent the burner outlet.

frequency of external perturbations. This contrasts strikingly with the absence of any scale-free structure in pressure networks formed under identical forcing conditions [Figs. 2(b4) and 2(b5)].

3. Thermoacoustically self-excited state

When the system is thermoacoustically self-excited (Fig. 6), the peak values of $|\omega|$ and s increase by an order of magnitude relative to the first two states (Secs. III B 1 and III B 2). These increases can be attributed to the two-orders-of-magnitude increase in $|p'|$ (Fig. 2). The stronger pressure oscillations give rise to more energetic vortical structures, both in the outer shear layers as well as in the central recirculation zone (Fig. 6). Crucially, the node strength distributions of the vortical networks exhibit a familiar power-law scaling with $-3 < \gamma < -2$ at nearly all times, regardless
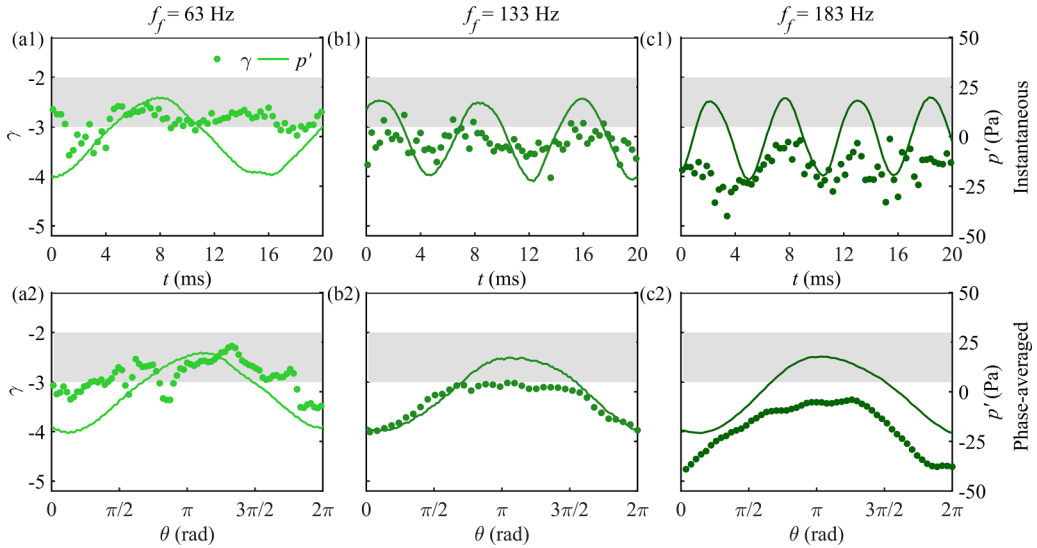
FIG. 5. Forced state without thermoacoustic instability (Re = 2600, $\phi = 0.8$): simultaneous evolution of γ and p' at three different forcing frequencies ($f_f = 63$, 133, and 183 Hz), but the same forcing amplitude ($u'/\bar{u} = 0.2$). The top and bottom rows show the instantaneous and phase-averaged data, respectively. For the phase-averaged data, a phase angle of 0 corresponds to the moment when an outer vortex ring is generated at the burner outlet.

of the phase of the oscillation cycle. This continuous scale-free behavior is in stark contrast to the intermittent scale-free dynamics observed in Fig. 5 for the forced state and in the studies by Murayama *et al.* [20] and Krishnan *et al.* [22] for thermoacoustically self-excited states. This shows that even after the onset of thermoacoustic instability, although scale-free topology disappears completely in the pressure networks [Figs. 2(c4) and 2(c5)], it survives robustly in the vortical networks [Figs. 6(c1)–6(c5) and Figs. 6(d1)–6(d5)].

The scale-free topology observed in the vortical networks can be explained through the flow physics. During thermoacoustic instability, it is generally recognized that large-scale vortical structures are responsible for most of the thermoacoustic driving—via the generation of large clusters of coherent acoustic power sources that act as the network hubs [22,36]. In turbulent combustors, such large-scale coherent vortices tend to coexist with many smaller incoherent eddies arising from the chaotic nature of the underlying turbulent flow field [1,27]. Consequently, the scale-free topology observed in the vortical networks can be attributed to the coexistence of two different classes of vortices: (i) a large number of vortices whose influence is mostly local, inducing only low-to-moderate flow velocities and forming network nodes with low-to-moderate s values, and (ii) a small number of vortices whose influence is global, inducing high flow velocities and forming network hubs with high s values. In our experiments, the latter class of vortices, corresponding to the primary network hubs, dominates the outer shear layers and their roll-up into vortex rings, as can be seen in the ω and s fields of Fig. 6. In summary, the coexistence of vortices of different interaction strengths is what physically causes scale-free topology to emerge in the vortical networks of this turbulent thermoacoustic system.

Although the topologies of the pressure and vortical networks are vastly different, we still find a strong degree of synchronicity between γ of the vortical networks and the p' signal itself. To illustrate this, we show in Fig. 7 the simultaneous evolution of γ, p', and $|\omega|$ at three different equivalence ratios: $\phi = 0.70$, 0.75, and 0.80. On increasing ϕ, we find that the amplitude of the thermoacoustic mode increases. This enhances the synchronicity of the γ and p' signals, as evidenced by an increase in their cross correlation (Fig. 7: CC = $0.58 \rightarrow 0.61 \rightarrow 0.82$). Meanwhile,
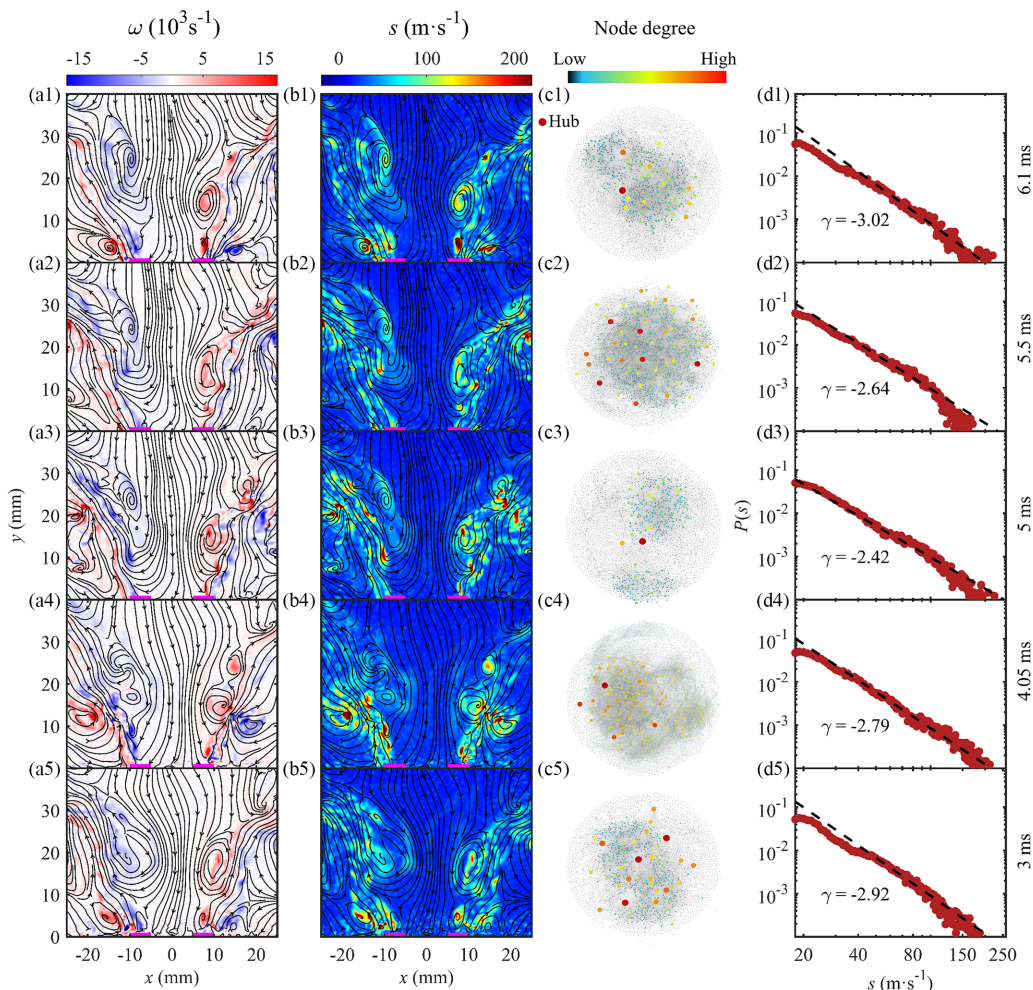
FIG. 6. Thermoacoustically self-excited state (Re = 6200, $\phi = 0.8$): (a1)–(a5) vorticity field, (b1)–(b5) node strength field from vortical networks, (c1)–(c5) network structure with the highest strength nodes (hubs) shown as red dots, and (d1)–(d5) node strength distribution on a log-log plot. The data shown are instantaneous, extracted at five instants in a natural oscillation cycle (see labels on the right). The time separation is around $\pi/2$. In the spatial data [(a1)–(a5), (b1)–(b5)], the black lines are streamlines and the magenta lines at the bottom represent the burner outlet.

the amplitude of the γ fluctuations increases as well, but not beyond the range $-3 < \gamma < -2$, implying that scale-free topology is continuously maintained in the vortical networks, even though it has disappeared completely in the pressure networks [Figs. 2(c4) and 2(c5)]. As with the forced state (Sec. III B 2), we find that γ fluctuates in time with the development of the coherent flow structures (Fig. 6), with moments of high γ coinciding with moments of high $|\omega|$ concentration (Fig. 7).

IV. CONCLUSIONS

We have investigated the vortical interactions in a bluff-body stabilized swirling combustion system via the construction of time-varying weighted spatial turbulence networks whose node strength distribution is derived from the Biot-Savart law. We focused on three canonical states: (i) an
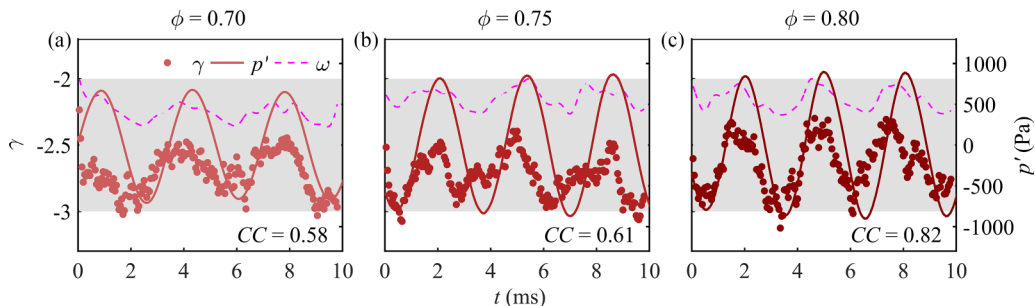
FIG. 7. Thermoacoustically self-excited state (Re = 6200): simultaneous evolution of γ, p', and maximum $|\omega|$ at three different equivalence ratios ($\phi = 0.70$, 0.75, 0.80). The $|\omega|$ data are included for qualitative comparison only, so their axis values are not displayed.

unforced state of combustion noise, (ii) an acoustically forced state without thermoacoustic instability, and (iii) a thermoacoustically self-excited state with limit-cycle dynamics. In all three states, we found evidence of hubs in the network structure and a power-law scaling in the node strength distribution, indicating the existence of scale-free topology. The scale-free topology appears nearly continuously in time for the unforced and self-excited states, but only intermittently for the forced state, depending on the exact forcing frequency. The coherent flow structures with strong vorticity were found to act as the primary network hubs, dictating the spatiotemporal dynamics of the entire flow. Murayama *et al.* [20] and Krishnan *et al.* [22] have shown that even during thermoacoustic instability, such scale-free topology can appear in vortical networks, but only intermittently. Here we have provided evidence that such scale-free topology can appear continuously in time in vortical networks, despite being completely absent in the corresponding pressure networks. This discovery sheds light on the robustness of the primary network hubs and may have implications for the efficacy of controlling self-excited thermoacoustic systems via external forcing directed at such network hubs [27].

[1] T. C. Lieuwen, *Unsteady Combustor Physics* (Cambridge University Press, Cambridge, 2012).

[2] S. Candel, D. Durox, T. Schuller, J. F. Bourgouin, and J. P. Moeck, Dynamics of swirling flames, Annu. Rev. Fluid Mech. **46**, 147 (2014).

[3] Y. Huang and V. Yang, Dynamics and stability of lean-premixed swirl-stabilized combustion, Prog. Energy Combust. Sci. **35**, 293 (2009).

[4] S. Candel, Combustion dynamics and control: Progress and challenges, Proc. Combust. Inst. **29**, 1 (2002).

[5] T. Poinsot, Prediction and control of combustion instabilities in real engines, Proc. Combust. Inst. **36**, 1 (2017).

[6] R. Balachandran, B. Ayoola, C. Kaminski, A. Dowling, and E. Mastorakos, Experimental investigation of the nonlinear response of turbulent premixed flames to imposed inlet velocity oscillations, Combust. Flame **143**, 37 (2005).

[7] P. Palies, D. Durox, T. Schuller, and S. Candel, The combined dynamics of swirler and turbulent premixed swirling flames, Combust. Flame **157**, 1698 (2010).

[8] K. Oberleithner, S. Schimek, and C. O. Paschereit, Shear flow instabilities in swirl-stabilized combustors and their impact on the amplitude dependent flame response: A linear stability analysis, Combust. Flame **162**, 86 (2015).

[9] M. Gatti, R. Gaudron, C. Mirat, L. Zimmer, and T. Schuller, Impact of swirl and bluff-body on the transfer function of premixed flames, Proc. Combust. Inst. **37**, 5197 (2019).

[10] M. Barthélemy, Spatial networks, Phys. Rep. **499**, 1 (2011).

[11] A. L. Barabási, The network takeover, Nat. Phys. **8**, 14 (2012).

[12] K. Taira and A. G. Nair, Network-based analysis of fluid flows: Progress and outlook, Prog. Aerosp. Sci. **131**, 100823 (2022).

[13] A. L. Barabási and R. Albert, Emergence of scaling in random networks, Science **286**, 509 (1999).

[14] A. L. Barabási, *Network Science* (Cambridge University Press, Cambridge, 2016).

[15] Z. K. Gao, M. Small, and J. Kurths, Complex network analysis of time series, Europhys. Lett. **116**, 50001 (2016).

[16] M. Murugesan and R. I. Sujith, Combustion noise is scale free: Transition from scale free to order at the onset of thermoacoustic instability, J. Fluid Mech. **772**, 225 (2015).

[17] Y. Okuno, M. Small, and H. Gotoda, Dynamics of self-excited thermoacoustic instability in a combustion system: Pseudo-periodic and high-dimensional nature, Chaos **25**, 043107 (2015).

[18] M. Murugesan and R. I. Sujith, Detecting the onset of an impending thermoacoustic instability using complex networks, J. Propul. Power **32**, 707 (2016).

[19] J. Tony, E. A. Gopalakrishnan, E. Sreelekha, and R. I. Sujith, Detecting deterministic nature of pressure measurements from a turbulent combustor, Phys. Rev. E **92**, 062902 (2015).

[20] S. Murayama, H. Kinugawa, I. T. Tokuda, and H. Gotoda, Characterization and detection of thermoacoustic combustion oscillations based on statistical complexity and complex-network theory, Phys. Rev. E **97**, 022223 (2018).

[21] K. Taira, A. G. Nair, and S. L. Brunton, Network structure of two-dimensional decaying isotropic turbulence, J. Fluid Mech. **795**, R2 (2016).

[22] A. Krishnan, R. I. Sujith, N. Marwan, and J. Kurths, Suppression of thermoacoustic instability by targeting the hubs of the turbulent networks in a bluff body stabilized combustor, J. Fluid Mech. **916**, A20 (2021).

[23] S. Murayama and H. Gotoda, Attenuation behavior of thermoacoustic combustion instability analyzed by a complex-network-and synchronization-based approach, Phys. Rev. E **99**, 052222 (2019).

[24] T. Kurosaka, S. Masuda, and H. Gotoda, Attenuation of thermoacoustic combustion oscillations in a swirl-stabilized turbulent combustor, Chaos **31**, 073121 (2021).

[25] S. A. Pawar, A. Seshadri, V. R. Unni, and R. I. Sujith, Thermoacoustic instability as mutual synchronization between the acoustic field of the confinement and turbulent reactive flow, J. Fluid Mech. **827**, 664 (2017).

[26] Y. Guan, L. K. B. Li, B. Ahn, and K. T. Kim, Chaos, synchronization, and desynchronization in a liquid-fueled diffusion-flame combustor with an intrinsic hydrodynamic mode, Chaos **29**, 053124 (2019).

[27] R. I. Sujith and S. A. Pawar, *Thermoacoustic Instability*, Series in Synergetics (Springer Nature, Switzerland, 2021).

[28] G. Wang, X. Liu, S. Wang, L. Li, and F. Qi, Experimental investigation of entropy waves generated from acoustically excited premixed swirling flame, Combust. Flame **204**, 85 (2019).

[29] J. Zheng, S. Wang, Z. Yang, L. Li, G. Wang, Y. Gao, X. Liu, and F. Qi, Experimental investigations on coherent flow structures in acoustically excited swirling flames using temporally-separated dual-plane stereo-PIV, Expt. Therm Fluid Sci. **136**, 110673 (2022).

[30] L. Xu, J. Zheng, G. Wang, Z. Feng, X. Tian, L. Li, and F. Qi, Investigation on the intrinsic thermoacoustic instability of a lean-premixed swirl combustor with an acoustic liner, Proc. Combust. Inst. **38**, 6095 (2021).

[31] B. Luque, L. Lacasa, F. Ballesteros, and J. Luque, Horizontal visibility graphs: Exact results for random time series, Phys. Rev. E **80**, 046103 (2009).

[32] A. Nuñez, L. Lacasa, E. Valero, J. P. Gómez, and B. Luque, Detecting series periodicity with horizontal visibility graphs, Intl. J. Bifurcat. Chaos **22**, 1250160 (2012).

[33] S. Murayama, K. Kaku, M. Funatsu, and H. Gotoda, Characterization of dynamic behavior of combustion noise and detection of blowout in a laboratory-scale gas-turbine model combustor, Proc. Combust. Inst. **37**, 5271 (2019).

[34] G. Wang, X. Liu, X. Xia, S. Wang, and F. Qi, Dynamics of periodically-excited vortices in swirling flames, Proc. Combust. Inst. **38**, 6183 (2021).

[35] P. Huerre and P. A. Monkewitz, Local and global instabilities in spatially developing flows, Annu. Rev. Fluid Mech. **22**, 473 (1990).

[36] A. Krishnan, R. I. Sujith, N. Marwan, and J. Kurths, On the emergence of large clusters of acoustic power sources at the onset of thermoacoustic instability in a turbulent combustor, J. Fluid Mech. **874**, 455 (2019).